



## *Decadal Climate and Global Change Research*



---

*The Climate Diagnostics Center contributes to understanding the variations in Earth's climate system on decadal to centennial time scales. Research includes process and model simulation studies to elucidate the relation between changes in the atmosphere and those in the ocean. CDC scientists seek to provide physical and dynamical understanding of observed long term climate variations and change through analysis of hierarchies of designed GCM experiments. These include atmospheric models forced by SSTs, ocean models forced by wind stress, and coupled ocean-atmosphere GCMs, including runs forced by greenhouse gases.*

*Our investigations have focused on determining fundamental processes responsible for decadal climate variability and change, and assessing whether the latter are due to human influences or natural variability. According to the Third Assessment Report of the IPCC, it is now very likely that global temperatures during the 1990s were the highest since 1861. The same appears to be true for tropical sea surface temperatures, and the areal coverage of the so-called oceanic warm pool (SSTs > 28.5°C) (**Fig. 5.1, top**). CDC scientists are diagnosing relationships between this tropical ocean warming, the global atmospheric circulation and recent climate change.*

*CDC is engaged in understanding how slow changes in climate affect interannual variability. One key question is determining whether the warm pool change over the equatorial west Pacific impacts the statistics of El Niño/Southern Oscillation (ENSO) in the eastern Pacific. It is evident that the strongest El Niño events in the instrumental record have occurred in recent decades (**Fig. 5.1, middle**); we are assessing if this is a signature of climate change or merely random fluctuations. The global impacts of ENSO have also changed in recent decades. A fundamental question being pursued at CDC is whether the ENSO teleconnections diagnosed from historical data of the 19th and 20th centuries will be accurate depictions of ENSO impacts in this new, unique century of human induced climate change.*

*CDC scientists are also studying the origin and climatic impact of midlatitude ocean changes. Most dramatic among these is the multi-decadal variability in SSTs over the Pacific poleward of 30°N (**Fig. 5.1, bottom**), an index of which has been termed the Pacific-Decadal Oscillation (PDO). The apparent long time scale of this oceanic behavior is quite different from that of the ENSO time series. Nonetheless, our analysis shows a strong relation between the two on interannual time scales, and an intriguing question is the extent of their coupling on multi-decadal scales. Likewise, the low frequency variations of North Pacific SSTs since 1950 have atmospheric counterparts, including changes in the oceanic storm track and the strength of the upper tropospheric westerly jet. CDC scientists are studying the nature of air-sea interaction over the North Pacific, and assessing to what extent the diagnostic relations mentioned above entail predictability.*

---

### **5.1 Modeling studies of low frequency atmospheric variability and climate change**

#### *5.1.1 Atmospheric circulation change and the role of tropical SST warming*

A significant component of global surface temperature trend since 1950 is

linked with planetary scale changes in atmospheric wind and pressure patterns, and our analysis based on atmospheric GCM experiments indicates that the latter have been forced by changes in tropical SSTs. During northern winter, the trend in 500-mb heights since 1950 consists of a uniform tropical and subtropical height increase, and a wavy pattern of

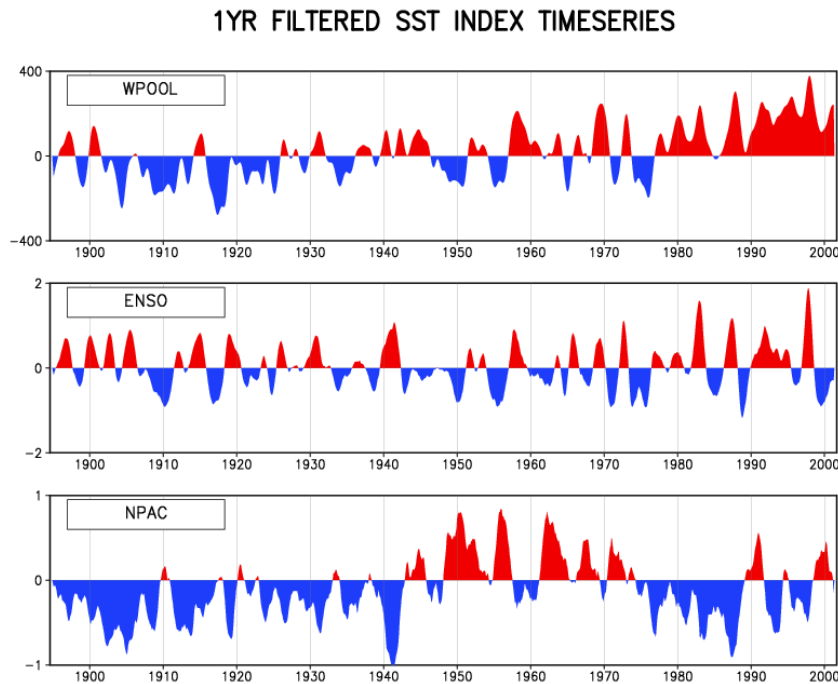


**Fig. 5.1.** (a) Warm pool index that describes the time series of areal coverage (expressed as the number of  $2^\circ$  by  $2^\circ$  grid boxes) of  $SST > 28.5^\circ\text{C}$  within the region ( $30^\circ\text{N}$ – $30^\circ\text{S}$ ,  $50^\circ\text{E}$ – $120^\circ\text{W}$ ). (b) Cold tongue index of ENSO that described the time series of area-averaged SST anomalies within the region ( $5^\circ\text{N}$ – $5^\circ\text{S}$ ,  $160^\circ\text{E}$ – $80^\circ\text{W}$ ). (c) North Pacific SST index for the area average within the region ( $30^\circ\text{N}$ – $50^\circ\text{N}$ ,  $150^\circ\text{E}$ – $150^\circ\text{W}$ ). All time series are for January 1895–April 2001, and have been smoothed with a 13-month running mean. The warm pool index is derived from GISST 2.3b data. The ENSO and North Pacific SST indices use the Kaplan data for 1895–1949, Smith and Reynolds reconstructed SST data from 1950–1981, and the Reynolds OI data after 1982. Anomalies are computed relative to the entire 107 year period.

stationary wave change in higher latitudes highlighted by lower pressure over the North Pacific and North Atlantic (**Fig. 5.2, top**). The change in the latter region projects strongly on the North Atlantic Oscillation (NAO) structure of monthly variability. Recent hypotheses for the North Atlantic climate change include a positive feedback resulting from coupling with North Atlantic SSTs, and the possibility that the slow variations are nothing more than sampling artifacts of a random stationary process. Earlier studies of North Pacific climate change have also argued for forcing from the slow variations in extratropical (North Pacific) SSTs (see **Fig. 5.1**),

together with forcing from changes in the tropical Pacific ocean. We have analyzed data from a 12-member ensemble of atmospheric simulations with NCAR's CCM3, using global SST variations since 1950, and these confirm that the observed circulation pattern trends are consistent with global air-sea interactions (**Fig. 5.2, middle**). The role of tropical SSTs is revealed from another GCM ensemble in which monthly SST variations are prescribed over only the  $30^\circ\text{N}$ – $30^\circ\text{S}$  band. That the observed trend is captured by the tropically forced simulations (**Fig. 5.2, bottom**) alone suggests that the gradual warming of those waters since 1950 is forcing NH climate change.

In fact, further analysis suggests that the secular warming within the oceanic warm pool region itself is most relevant for the simulated climate change, particularly over the distant North Atlantic sector.

Tropical SST warming since 1950 has altered tropical rainfall, the likely immediate cause for the simulated atmospheric circulation changes. The modeled rainfall trend is consistent with that of the underlying SSTs, with increased precipitation throughout the entire equatorial Indo-Pacific region (**Fig. 5.3, top**). This leads to the question of the origin of the tropical SST change itself (**Fig. 5.3, bottom**). Analysis of coupled ocean-atmosphere experiments indicate that the warming trend is beyond the range of natural variability. The changes do appear consistent with anomalous greenhouse forcing, however, insofar as the pattern and amplitude of warming during the past half century is similar to that predicted by such models when forced by observed greenhouse gas changes. Our current working hypothesis is that the spatial pattern of NH winter climate change, and the regional change over the North Atlantic/European sector especially, is being forced by a tropical ocean warming, and implicitly reflects an emergent anthropogenic signal.

### 5.1.2 Global warming and atmospheric angular momentum

The recent trends in wintertime NH height are strongly annular from the surface to the lower stratosphere. Heights have been increasing in the tropics but

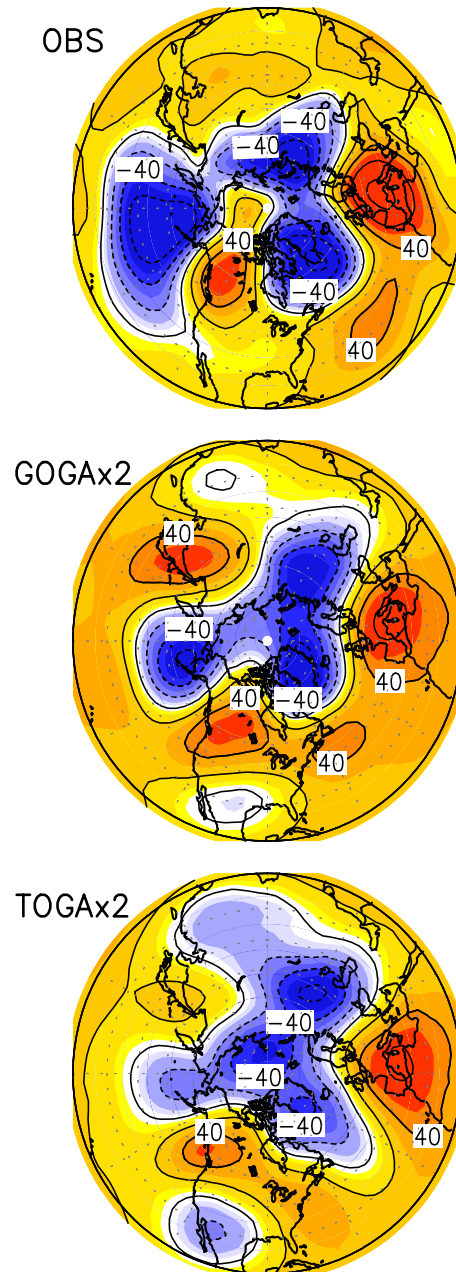


**Fig. 5.2.** The linear trend of the winter season (December to February) 500-mb height field based on observations (top), 12-member CCM3 ensemble forced by global SST variations (middle), and 12-member CCM3 ensemble forced by tropical SST variations over 1950-1999 (bottom). The model results have been multiplied by a factor of 2. Height increases (decreases) are indicated by solid (dashed) contours, and the contour increment is 20 m per 50 years. (Based on results of Hoerling, Hurrell and Xu, 2001, *Science*).

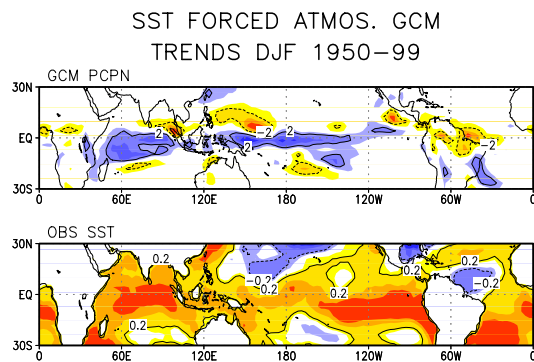


**Fig. 5.3.** The linear trend of the winter season (December to February) total precipitation from the 12-member CCM3 ensemble forced by tropical SST variations (top), and the observed sea surface temperatures (bottom). (Based on results of Hoerling, Hurrell and Xu, 2001, *Science*).

decreasing near the poles, and associated with this has been an increase in the atmospheric angular momentum (AAM) (**Fig. 5.4**). Much of the increase reflects a change in relative angular momentum that is due to a broad westerly wind increase within 30°N–30°S. We have been seeking an explanation for this change using GCM simulations subjected to various forcings. First, the change of AAM was investigated in a three-member ensemble of coupled ocean-atmosphere model simulations

with increasing atmospheric greenhouse gases and sulfate aerosol loading for the period 1900–2100. A highly significant increase in total AAM was found to occur in those runs, with an indication that the forced change emerges above the noise of natural variability by the late 20th Century.

We hypothesize that the AAM is responding to SST changes and accompanying tropical convection, rather than to direct changes in radiative forcing. In the model, the AAM is found to accompany an increase in tropical SST with a sensitivity of  $\sim 1$  AMU/°C (1 AMU =  $10^{25}$  kg m<sup>2</sup> s<sup>-1</sup>). A similar sensitivity is found in the observed AAM response to Niño 3.4 SSTs during El Niño. To further examine the role of SST changes only, we analyzed a 12-member ensemble of NCAR CCM3 simulations forced with the history of global SSTs during 1950–99. The simulated AAM from these runs compares well with the time history of the (single realization) observed AAM, and with the observed trend in Niño 3.4 SSTs (see **Fig. 5.4**). The AAM time

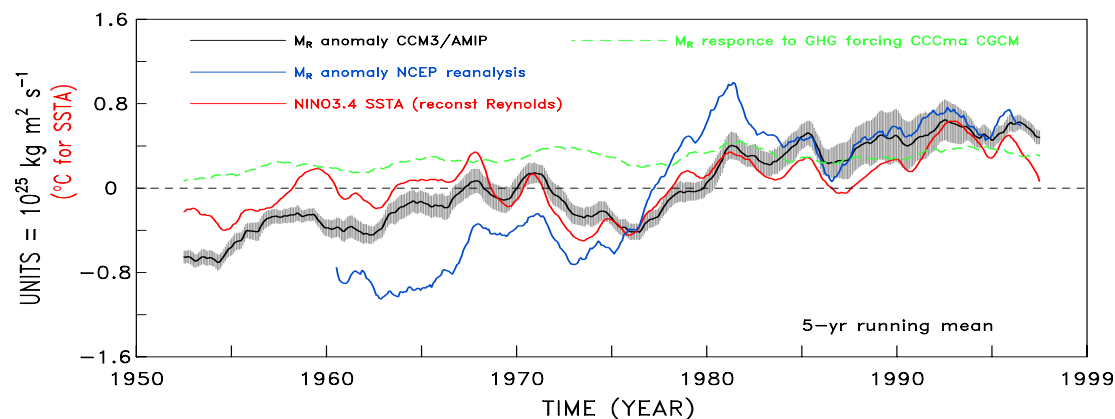


**Fig. 5.4.** Time series of global angular momentum from 1950–1999 based on NCEP/NCAR reanalysis (blue), 12-member CCM3 ensemble forced with global SST variations (black), Canadian Centre for Climate Modeling coupled GCM forced by greenhouse gases and aerosols (green). The standard deviation among the CCM3 ensemble members shown in shading. The time series of Niño 3.4 SSTs is shown in red. All curves smoothed with a 5-yr running mean. (Based on results of Huang, Weickmann and Hsu, 2001, *J. Climate*, in press).

series in the greenhouse forced experiment also shows an increasing trend, though it appears to underestimate the observed low frequency variability. All four curves show a trend during 1950–99 of approximately the same magnitude, although the coupled run has the smallest and the observed AAM has the largest trend. The curves cluster together after 1980, while before that time the AMIP ensemble lies between the coupled ensemble and the observed curve. The implication is that the observed AAM trend is partially the result of global warming, through its effect on the tropical heat sources, although natural variability (and NCEP reanalysis errors) probably also contribute. In any case, the anthropogenic forced change through 1999 is as yet modest, especially compared to the AAM change predicted to

occur by this model over the next 100 years ( $\sim 4$  AMU).

### 5.1.3 Decadal variations in ENSO and its global impact

Observations reveal that the global impacts of ENSO vary substantially on decadal time scales. One example is the breakdown in the ENSO-Indian monsoon relationship in the last quarter century. In addition to such changes in tropical teleconnections, ENSO's extratropical impacts have also shown strong decadal variations. For example, ENSO has explained a much higher fraction of the seasonal atmospheric variability in the PNA-sector since 1977 compared to the prior quarter century. The February–April seasonal correlation of 500-mb heights with a SST index of ENSO has roughly

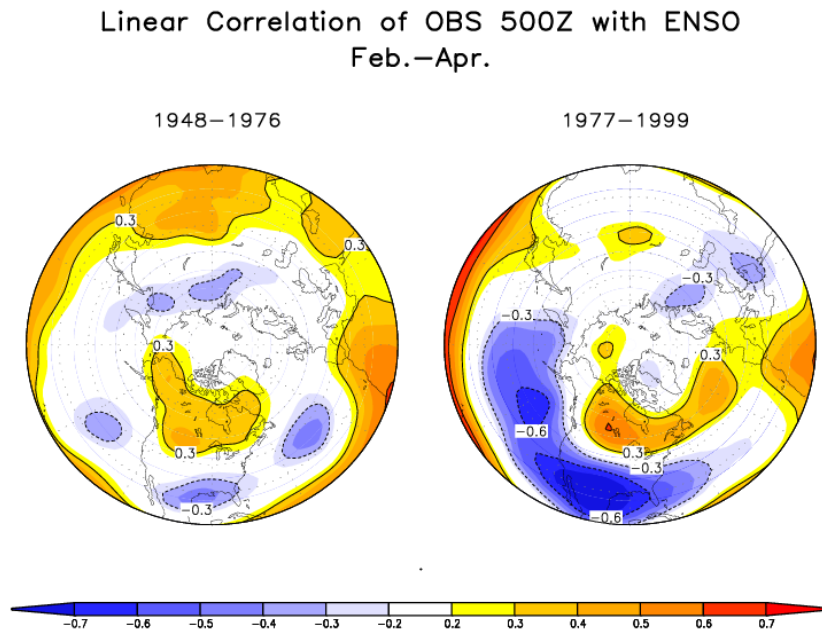


**Fig. 5.5.** Correlation pattern of seasonally averaged February–April 500 hPa geopotential height with the ENSO index of the middle panel of Fig. 5.1 calculated for two sub-periods: 1948–1976 (left panel), and 1977–1999 (right panel). Results are shown for the Northern Hemisphere for the area extending north of 20 degrees latitude. (Based on results of Diaz, Hoerling and Eischeid, 2001, *Int. J. Climat.*, in press).

doubled during 1977–99 compared to 1948–76 (**Fig. 5.5**). The correlation, averaged across the southern US between  $120^{\circ}\text{W}$ – $70^{\circ}\text{W}$ , increases from roughly  $-0.2$  to  $-0.6$  in the recent period, and points to a substantial increase in the late-winter potential predictability.

One might suppose that this change in predictability is due to the stronger ENSO forcing as measured by the increased interannual variance of tropical Pacific SSTs since 1977 (see **Fig. 5.1**). Yet, this increase is only about 20 percent, and it is not reconcilable with the much greater fractional increase in variance of the remote ENSO signal. Recent changes in the life cycle of tropical Pacific SST anomalies during warm

events may be a key factor. The so-called canonical warm event evolution prior to 1977, using the cases of Rasmusson and Carpenter, had peak warming in December, followed by rapid decay (**Fig. 5.6, left panel contours**). We have calculated the difference in SST lifecycles between the post-1977 and pre-1977 warm events (**Fig. 5.6, left panel shading**), and found that recent cases prolong their warming into spring of year+1, and also defer South American coastal warming until spring of year (+1). This change is relevant for the teleconnections because the recent warm events peak closer to the peak in climatological warming of the east equatorial Pacific ocean, so that the total SST is actually now maximized in spring of year+1 rather than in early win-

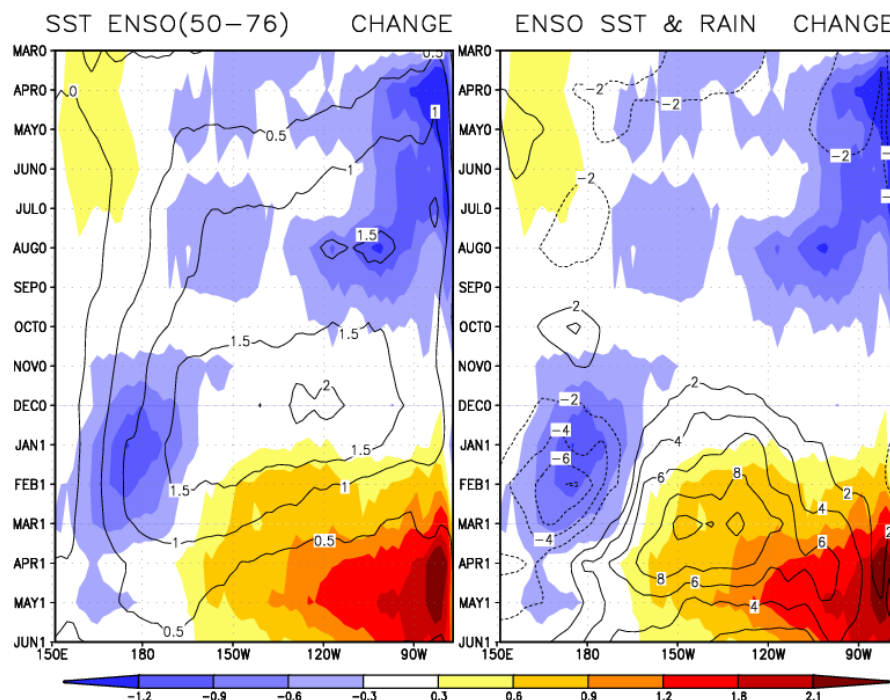


**Fig. 5.6.** Hovmuller diagrams illustrating the change in the composite life cycle of SST and rainfall anomalies along the equatorial Pacific during 1948–1999. In the left panel, contours illustrate the composite El Niño SST anomaly based on pre-1976 events, whereas the shading illustrates the difference in El Niño SST composites for events occurring after versus before 1976. In the right side panel, the contours illustrate the change in El Niño rainfall anomaly composites for events occurring after versus before 1976, as derived from climate simulations. The shading repeats the SST change of the left panel. (Based on results of Diaz, Hoerling and Eischeid, 2001, *Int. J. Climat.*, in press).

ter. Using output from AMIP-style simulations spanning 1950–99, we have found a large increase in rainfall for the post-1977 events relative to the pre-1977 events (**Fig. 5.6, right panel contours**) that corresponds closely with the change in SSTs. The change in composite rainfall represents a doubling relative to the pre-1977 cases, suggesting that the recent teleconnection strength is at least qualitatively consistent with a secular change in tropical forcing, though other factors may also be involved.

## 5.2 Modeling studies of fundamental ocean processes

From the various atmospheric GCM experiments described above, two aspects of tropical ocean change in the 20th Century have been implicated as forcing observed atmospheric change; *i*) the warming of the warm pool region and *ii*) the nonstationarity of the ENSO time series. Our research on fundamental ocean processes leads to the hypothesis that these two oceanic changes are themselves coupled, and in particular that the recent increase in El Niño amplitude is consistent with the increase in warm pool temperature.

### 5.2.1 Decadal ENSO variability and the role of warm pool SST

From detailed analysis of the 1986–87 El Niño event, we find that El Niño represents a mechanism by which the equatorial Pacific transports heat poleward, a result subsequently confirmed from a more extended study using NCEP data for the last 20 years. In particular, a sys-

tematic relationship between the ocean heat content in the western Pacific and the magnitude of El Niño warming was diagnosed for six events since 1980—the higher the heat content in the western Pacific, the stronger the subsequent El Niño warming (**Fig. 5.7, top**). The occurrence of warm pool heat content maxima,

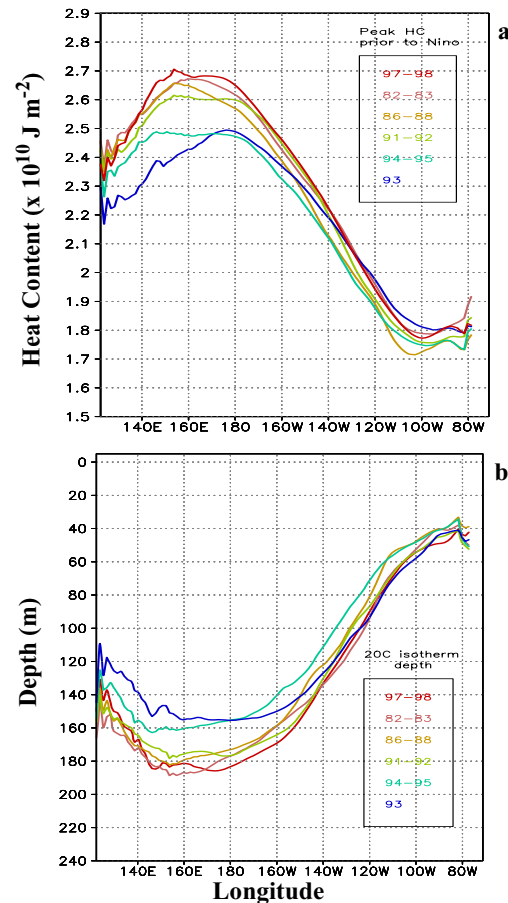


**Fig. 5.7.** (a) Zonal distribution of upper ocean heat content (0–260 m) in the equatorial belt (5°S–5°N) when the western Pacific heat content reaches its pre-El Niño peak. Upper ocean heat content used for this figure was smoothed in time using a Hanning window with a width of 13 months. (b) The corresponding depth of the 20°C isotherm. The ocean temperature used for calculating the 20°C isotherm depth was smoothed in time using a Hanning window with a width of 13 months. (Based on results from Sun 2001, *J. Climate*, submitted).

at which time the zonal cross sections of **Fig. 5.7** were made, precede the maxima in Niño 3 SST anomalies by 12–24 months.

Our interpretation is that higher heat content in the western Pacific is achieved through a deepening of the local thermocline, thus linking the heat content in the western Pacific to the potential energy of the ocean and thereby with the stability of the coupled ocean-atmosphere system (**Fig. 5.7, bottom**). As warm-pool SST initially increases, the zonal SST contrast also increases, strengthening the trade winds. The stronger Walker circulation then interacts with clouds and water vapor, allowing more solar radiation to reach the ocean's surface over the east Pacific equatorial cold-tongue, and at the same time, reducing the surface evaporative cooling over that region. This is so because the impact of change in the gradient term of the latent heat flux formula exceeds the impact of increased wind speed. Through non-local ocean wave dynamics and transports, heat content increases in the equatorial upper ocean of the western Pacific warm pool. The resulting steeper tilt of the equatorial thermocline is hypothesized to destabilize the coupled system which is followed by energy release through a stronger El Niño.

To test this hypothesis, we constructed a coupled model. The atmospheric model is statistical, with the equatorial surface winds proportional to the zonal SST gradients. The ocean component is a primitive equation model and therefore explicitly calculates the heat budget of the entire equatorial upper ocean. The

model produces ENSO-like variations. The evolution of the subsurface ocean temperature over the life cycle of the model El Niño resembles that of observations (**Fig. 5.8**). In response to an increase in warm pool SST, the model has a stronger El Niño. Similar to the observational results, this simple model shows that an increase in warm pool SST strengthens the zonal SST contrast during ENSO's cold phase, which leads to an effective increase in the upper ocean heat content in the warm pool. Stronger El Niño warming then follows, which acts as a poleward heat pump. Of course, other processes can operate to increase warm pool SSTs. In regard to the observed recent climate change (see **Fig. 5.1**), it is reasonable that the warm pool has increased due to local radiative forcing related to the increase in anthropogenic gases. It is hypothesized that this externally forced change may be influencing the statistics of ENSO through the mechanisms described above.

### *5.2.2 North Pacific decadal ocean variability and the role of the tropics*

As mentioned earlier, the time series of the ENSO index is correlated with that of North Pacific SSTs (see **Fig. 5.1**), despite their different time scales of variation. This reflects in part the well-known fact that ENSO influences the North Pacific circulation, which in turn forces North Pacific SSTs, on interannual time scales. The question we have pursued is to what extent this atmospheric bridge between the tropics and extratropics contributes to the decadal variability over the North Pacific, including the Pacific Decadal Oscillation? We have addressed this

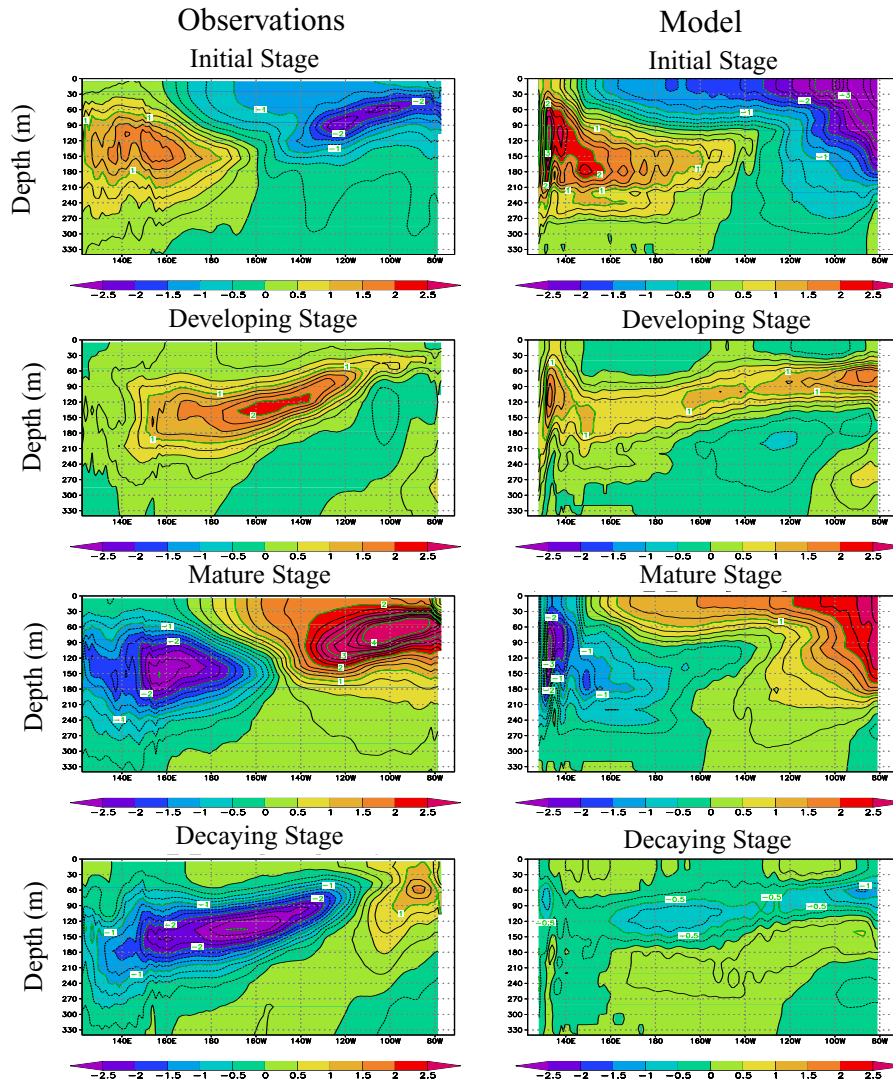


**Fig. 5.8.** The observed (left panels) and coupled model simulated (right panels) ocean temperature anomalies during an El Niño event's life cycle. Vertical sections are from surface to 330 m. Warm (cold) anomalies in red (blue). Observations based on El Niño composite during 1980–1999 based on NCEP ocean analysis. (Based on results from Sun 2001, *J. Climate*, submitted)

question by comparing the observed and simulated leading pattern (EOF 1) and associated principal component time series (PC) of wintertime North Pacific decadal SST variability (**Fig. 5.9**). The model results are obtained from the ensemble average of 16 50-year GFDL R30 AGCM simulations in which

observed SSTs are specified in the tropical Pacific over the period 1950–1999 and a mixed layer model (MLM) is coupled to the AGCM elsewhere over the global oceans. The EOFs are based on the monthly SST anomalies that were first low-pass filtered to retain periods greater than ~10 years and then the fil-

tered values from November to March were averaged together. The observed and MLM EOFs resemble each other in several respects: they both explain about half of the variance, and they are relatively well correlated in space and time, with a spatial (temporal) correlation of 0.71 (0.69). The patterns in **Fig. 5.9** are very similar to those based on unfiltered data which has conventionally been used to define the PDO. The observed and simulated PCs are well correlated with the filtered ENSO index time series, with correlation values of 0.77 and 0.90, respectively. In addition, maps of SST differences centered on 1976 (e.g., 1977–1988 minus 1970–1976, and 1977–1998 minus 1951–1976; not shown) indicate that the “abrupt climate transition” in the model and observations are similar and resemble the leading EOF but the amplitude of the differences is approximately half as large in the MLM. Overall, our model results suggest that a significant fraction of the variance of the dominant pattern of low frequency SST variability in the North Pacific is associated with the atmospheric bridge.

### 5.2.3 Subduction and Rossby wave dynamics: mechanisms for decadal ocean variability

Dynamic ocean processes likely play a fundamental role in climate variability on decadal timescales. Rossby wave propagation can introduce multi-year delays in the oceanic response to changes in the atmospheric forcing. Subduction, where surface waters enter and flow within the permanent pycnocline, provide a link between the extratropical and tropical oceans over an ~8 year period. It

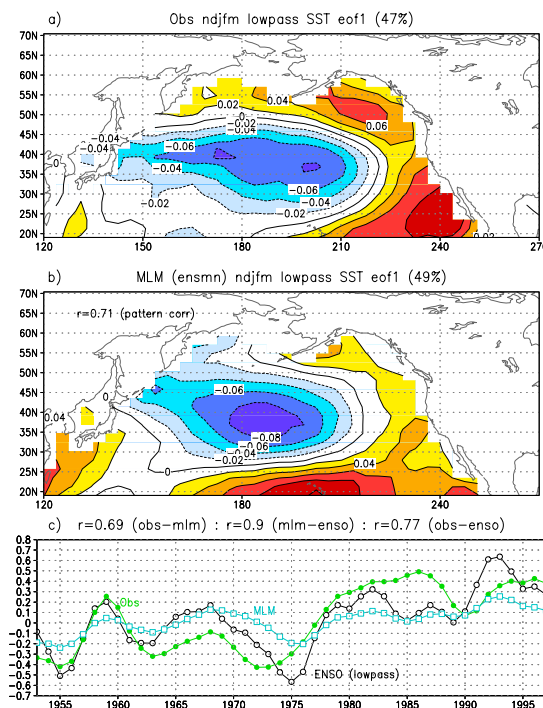


**Fig. 5.9.** EOF 1 of the low-pass filtered ( $> \sim 10$  years) SST anomalies during November–March from (a) observations and (b) the MLM. (c) The first principal component (time series associated with EOF 1) of the low-pass SST anomalies from observations (green line), the MLM (blue line) and low-pass ENSO index (black line). The correlations ( $r$ ) between the three time series are given above (c). (Based on the results of Alexander, Blade, Newman, Lau, and Lanzante, 2001, *J. Climate*, submitted).

has been conjectured that when the subducted anomalies reach the equator, they alter the equatorial SSTs and affect the North Pacific Ocean via the atmospheric bridge, completing a circuit that enables decadal oscillations. CDC has been involved in observational and modeling studies that examine subduction and Rossby waves in the Pacific Ocean.

The standard deviation of the depth of the  $25.5 \sigma_\theta$  isopycnal surface, obtained from a global OGCM forced by observed surface fluxes, indicates that there are three major centers of variability, includ-

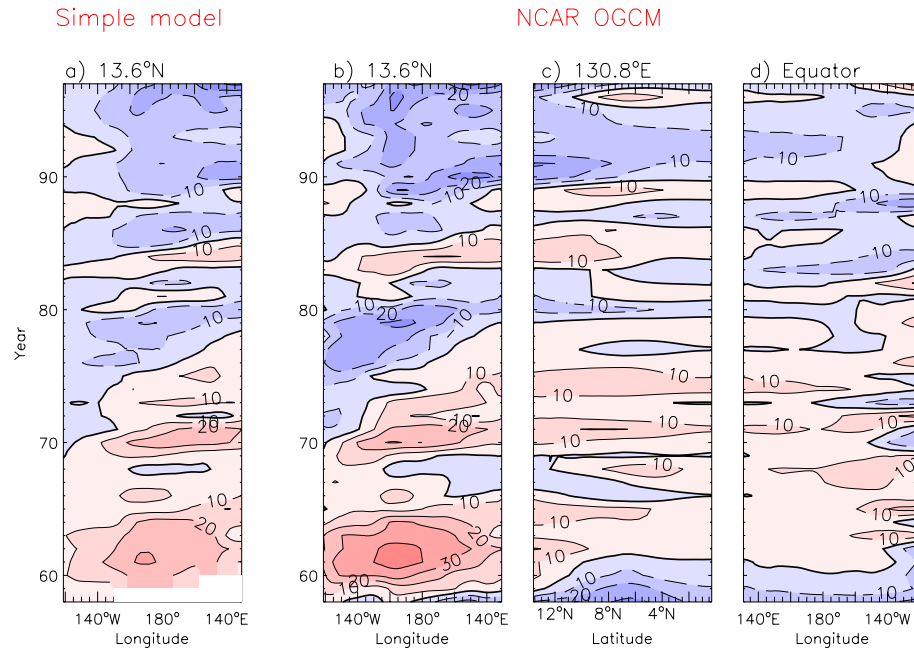


**Fig. 5.10.** (a) Evolution of the thermocline depth along  $13.6^{\circ}\text{N}$  (from east to west) as computed using a first-mode baroclinic Rossby wave equation forced with the Ekman pumping derived from the NCEP-NCAR reanalyses over the period 1958–1997. The equation was solved using the method of characteristics. Contour interval is 10 m. Negative values (shallower thermocline) are shaded in blue, while positive values (deeper thermocline) are shaded in red. (b) Same as in (a), but computed from the NCAR OGCM. The 25.5 isopycnal has been used as a proxy for thermocline depth. (c) Evolution of the depth of the 25.5 isopycnal along  $130.8^{\circ}\text{E}$  from  $13.6^{\circ}\text{N}$  to the equator. (d) Evolution of the depth of the 25.5 isopycnal along the equator, from east to west. In the OGCM anomalies originating along  $13.6^{\circ}\text{N}$  can be tracked all the way to the equator and along the equator. (Based on results of Capotondi and Alexander, 2001, *J. Phys. Oceanogr.*, in press).

ing: *i*) the Kuroshio region ( $30^{\circ}\text{N}$ ,  $160^{\circ}\text{E}$ ), *ii*) along the outcrop line at  $35^{\circ}\text{N}$  between  $180^{\circ}$ – $140^{\circ}\text{W}$ , and *iii*) the tropics between  $10^{\circ}\text{N}$ – $15^{\circ}\text{N}$ . The variability in the Kuroshio region reflects changes in the ocean thermal structure resulting from the basin-wide changes in the strength of the westerly winds that occurred in the late 1970s and late 1980s. The thermocline changes lag changes in the basin-wide wind stress curl forcing by 4–5 years, consistent with the timescale of oceanic adjustment through Rossby wave propagation. The second center of variability is associated with subduction, where it has been proposed

that thermal anomalies produced at the surface primarily by anomalous heat fluxes, propagate equatorward along isopycnals by the mean currents. Analyses of the OGCM and observations has allowed us to track thermal anomalies from their source region  $25^{\circ}\text{N}$ – $35^{\circ}\text{N}$ ,  $140^{\circ}\text{W}$ – $170^{\circ}\text{W}$  southwestward to  $\sim 18^{\circ}\text{N}$  over a period of  $\sim 8$  years. South of this latitude thermocline variability appears to be driven by local wind forcing.

The isopycnal depth changes in the subtropics of both hemispheres are associated with large thermocline temperature variations in both the OGCM and obser-

variations. We have examined the variability at  $10^{\circ}\text{N}$ – $15^{\circ}\text{N}$  by comparing the OGCM results with those obtained from a simple Rossby wave model forced by the same winds used in the OGCM simulation. The evolution of thermocline depth is remarkably similar in the simple model and OGCM (Fig. 5.10), indicating that a substantial portion of the variability in the  $10^{\circ}$ – $15^{\circ}\text{N}$  latitude band results from wind-forced baroclinic Rossby waves. Spectra and Hövmoller diagrams based on low-pass filtered OGCM output indicate that most of the thermocline variability occurs at periods longer than  $\sim 7$  years. East of the dateline, subtropical Ekman pumping anomalies exhibit variability over decadal periods and propagate westward at speeds close to the phase speed of first baroclinic mode Rossby waves. Thus, the spectral characteristics of the forcing may be responsible for the enhanced oceanic response at low frequencies. The thermocline signal that propagates across the basin at  $13^{\circ}\text{N}$ ,

moves southward along the western boundary and then eastward along the equator (see Fig. 5.10). The low-frequency variations of the thermocline depth along the equator may modulate the amplitude and period of ENSO events on decadal timescales, an outcome we plan to explore in the near future.

### 5.3. Empirical studies of decadal variability and climate change

#### 5.3.1 Observed change in the global hydrologic system

Interest in the potential impacts of climatic change in high elevation regions has grown in the past decade, as information from glacial monitoring sites and from fieldwork has demonstrated that significant melting and glacial recession has been occurring. Fifty-year trends in near-surface temperature (1948–2000) averaged over 5 different mountainous

Trend in Monthly Land Surface Area above Freezing Level

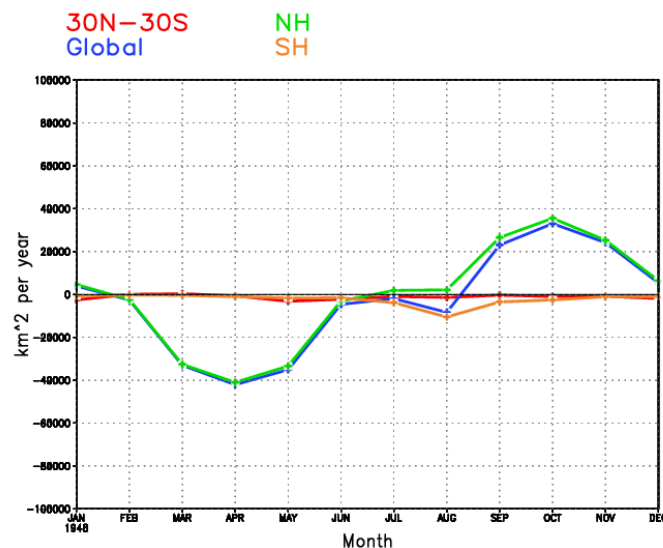


Fig. 5.11. The 1948–2000 linear trend in surface area above the freezing level surface (FLS) for the tropics, NH, SH, and globe for each calendar month. Data is the NCEP/NCAR reanalysis. (Based on a study by Diaz, Eischeid, Duncan and Bradley 2001).

regions are similar in magnitude to global temperature trends (+0.4–0.6 °C/50 yrs). We have been studying the relation between such behavior and changes in the land surface area located above the freezing level. The freezing level surface (FLS) is defined to be the 0°C isotherm, and the land area inside the roughly 2.5° lat/lon grid boxes of the NCEP/NCAR Reanalysis data that exceeds the FLS height was calculated monthly during 1948–2000. The most striking result is the strong seasonal dependency of trend in the land surface area above the freezing level, with largest decreases in spring consistent with a warming, but nearly equal increases in fall indicative of cooling (**Fig. 5.11**). Overall, the annual change reveals a small net decrease.

We are studying the impacts of climate change on a number of natural systems, including alpine hydrology and ecology, and the relevance for water resources management. A prominent feature of low frequency variability in streamflow has been the systematic change in timing of peak runoff over most of the globe since

1945 (**Fig. 5.12**). Peak flows are occurring earlier now than a half-century ago. This is particularly pronounced in river basins with a high fraction of their streamflow supplied by snowmelt, and reflects the springtime warming trend in these regions.

### 5.3.2 Secular change in North Pacific cyclone activity

The picture emerging from our GCM analyses of wintertime atmospheric trends since 1950 is of a relationship between changes in tropical SSTs and trend patterns in zonally averaged flow and planetary waves, in the sense that the former is forcing the latter. Given that the large scale circulation controls the statistics of sub-seasonal variations, such phenomena as the storm tracks and the transients that define them should also exhibit secular change. As one example, we have documented an increase in the frequency and strength of intense winter cyclones (minimum central pressure lower than 975 hPa) in the North Pacific Ocean since 1948 (**Fig. 5.13**). The time

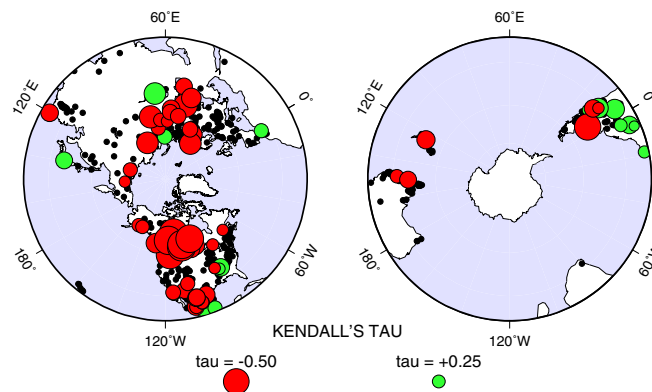


**Fig. 5.12.** Global trends in the time of streamflow during 1945–1993 as measured by the flow-weighted average day of flows in extratropical rivers. Red circles denote retrogression of the annual hydrograph. (Based on a study by Dettinger and Diaz, 2001).

series of December-March averaged counts of cyclones having a minimum pressure below 975 mb shows a substantial increase since 1948.

Associated with these changes are upward trends in extreme surface wind speeds between 25°–40°N, and an increase in significant wave heights. It is surmised that the cooling trend of North Pacific SSTs since 1950 (see Fig. 5.1) has in part been driven by the anomalous latent heat fluxes associated with this enhanced storminess. We also postulate that increasing sea surface temperatures in the western Pacific warm pool region (see Fig. 5.1) is a cause of the observed cyclone changes. The NCAR CCM3 simulations give some support for this premise, insofar as changes in the western Pacific warm pool and ENSO amplitude on decadal-scales impact the midlatitude stationary waves via teleconnection processes.

### 5.3.3 Decadal variations in summertime monsoons

Large summertime changes have occurred in tropical monsoon circulations since 1948 that are no less dramatic than the aforementioned low frequency variations in the wintertime ocean/atmosphere system. We already alluded to the secular change in ENSO's interannual impacts on Indian summertime monsoon rainfall. We have examined the mean change in the summertime monsoons since 1948 using the NCAR/NCEP re-analysis circulation data, together with station rainfall data where available. A prominent change has occurred in the divergent mass circulation describing the

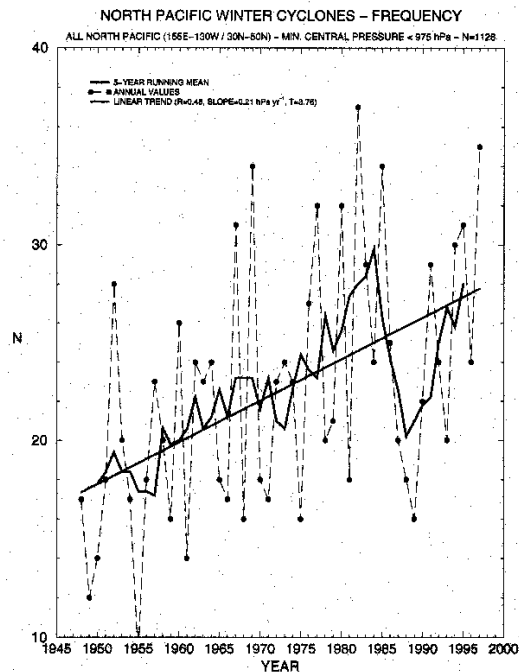


**Fig. 5.13.** Time series of the frequency of North Pacific winter cyclones having minimum sea level pressure < 975 mb during 1948–1997. The dark curve is the smoothed 5-yr point average, and the dark line is the linear trend. Data is the NCEP/NCAR reanalysis. (Based on results from Graham and Diaz, 2001, *Bull. Amer. Meteor. Soc.*, in press).

summer monsoons of both western and eastern hemispheres (Fig. 5.14, top). The maxima in the change map represent roughly 20 percent of the climatological mean. Station rainfall data allow us to verify that drying has indeed occurred over the Sahel in recent decades, consistent with the trend toward strong low level divergence (red shading) and implied sinking motion in the re-analysis data. We have yet to establish the realism of the re-analysis changes in the other summertime monsoons of Asia and the Americas, and a key hurdle in making sense of this picture is determining the fidelity in the re-analysis data itself, which is known to be biased by some spurious trends during 1948–2000.

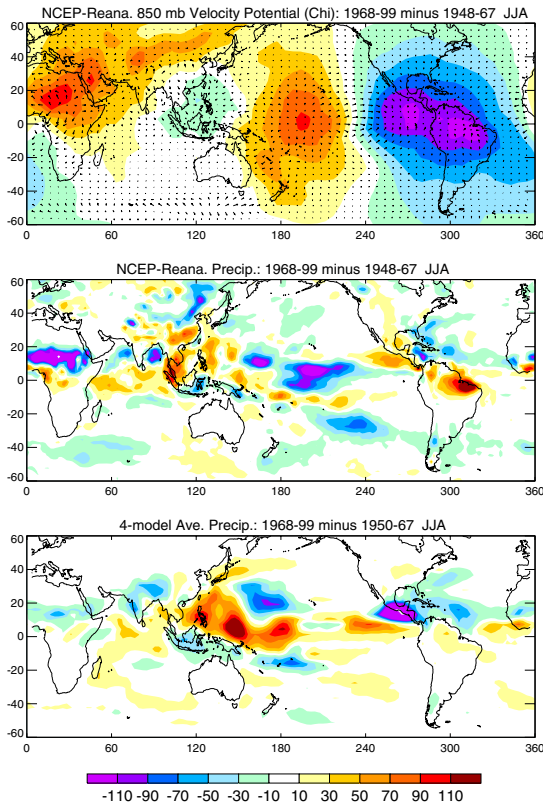


**Fig. 5.14.** Interdecadal change in the (top) 850mb velocity-potential ( $5 \times 10^6 \text{ m}^2 \text{ s}^{-1}$ ), (middle) precipitation ( $\text{mm month}^{-1}$ ) of the NCEP/NCAR reanalysis, and (bottom) precipitation of the average of four atmospheric general circulation models ( $0.3 \text{ mm month}^{-1}$ ). (Based on results of Quan, Diaz, and Fu, 2001, *J. Climate*, submitted).

To be sure, the re-analysis mass circulation changes are consistent with the re-analysis rainfall changes (compare top and middle panels of **Fig. 5.14**), and it is the origin of the latter which requires an explanation. We have begun to pursue the possibility that such apparent tropical-wide, low frequency changes in the atmosphere are reacting to a lower boundary SST change, perhaps akin to the wintertime change in tropical forcing discussed in earlier sections. The lower panel of **Fig. 5.14** shows the change in rainfall as derived from a multi-GCM

ensemble of AMIP-style simulations of 1950–1999. Rainfall has increased in the simulations over oceanic regions (red shading), especially the warm pool of the western Pacific and the Indian Ocean. This is in broad agreement with the re-analysis. Note also that the general drying (blue shading) over North Africa, Indonesia, and the Caribbean in re-analysis data emerges as a response pattern to SST. Our assessment is not complete, and we are pursuing various hypotheses motivated from our empirical study.

## EPILOGUE

It has become increasingly important to provide attribution for low frequency variations and change in Earth's climate. Whether this is for improved scientific understanding, predictability assessment, or to better inform societal planning and decision making, CDC is dedicating increasing resources to climate change research. At CDC, we seek to offer *dynamical explanations* for observed low frequency variations and change, thereby drawing strongly upon our expertise on seasonal to interannual variability, especially regarding air-sea interactions and teleconnective influences.

A key challenge that we will pursue in CDC is to understand and anticipate the *regional characteristics of climate change*. While there is now little question that the climate has changed in a globally and annually averaged sense, it is unclear what the local manifestations of this are, nor do we appreciate their seasonal dependencies. Beyond its relevancy to

long term planning, this problem is of high relevance to seasonal climate predictions. The fact is that the leading source of US winter temperature skill in the 1990's is due to the so-called optimal climate normals (OCN) tool, which we understand to be essentially a trend prediction. It is necessary that a physical explanation for such trends be given, and that they be clearly distinguished from low frequency climatic variations. Most apparent of these trends is the US wintertime surface warming, but other seasons show a more complicated pattern for temperature and rainfall change. We believe that progress can be made by improving our understanding of the regional responses to the slow, systematic changes in tropical oceans such as illustrated in **Fig. 5.1**, and we expect that much is to be gained from our existing knowledge of the interannual impacts of tropical forcing.

The change in the oceans itself is a problem that will focus future CDC decadal climate research. The mean change in ocean temperatures is a question that will require increased analysis of coupled ocean-atmosphere models. We expect to

partner with GFDL, NCAR and other interested scientists to diagnose and understand the variability in coupled model simulations, both natural and forced. We are especially interested in the sensitivity of ENSO to climate change, both its statistical properties and its interannual global impacts. A related challenge is to understand whether the year-to-year predictability of climate will change appreciably under the influence of human-induced mean change. Will ENSO as an oceanic phenomena become more predictable? Is it possible also that new regions will begin to have useful ENSO-related climate predictability? Likewise, we would like to understand whether the seasonal cycle of predictability will change due to an altered mean climate. These questions, among others, cut across time scales, and the greatest payoff in solving them may in fact be to advance key problems on shorter time scales, such as interannual prediction.

**Contributed by:** *M. Alexander, A. Capotondi, H. Diaz, M. Hoerling, H. Huang, X. Quan, D. Sun, and K. Weickmann.*